Deep spontaneous penetration of a water droplet into hot granular materials

Fangye Lin
Zhejiang University
Wei Wang
Zhejiang University
Stephane Dorbolo
university of liege
Jun Zou (junzou@zju.edu.cn)
Zhejiang University https://orcid.org/0000-0003-2443-3516

Article

Keywords: granular materials, droplets, vapour

Posted Date: December 9th, 2020

DOI: https://doi.org/10.21203/rs.3.rs-103868/v1

Deep spontaneous penetration of a water droplet into hot granular materials

Fangye Lin[1,2a], Wei Wang[2a], Stéphane Dorbolo[3*], and Jun Zou[2]**

[1]Ningbo Research Institute, Zhejiang University, Ningbo 315048, China
[2]State Key Laboratory of Fluid Power and Mechatronic Systems, Zhejiang University, Hangzhou 310027 China
[3]FNRS-CESAM-GRASP, Département de Physique, Université de Liège, Belgique
[a]The authors contributed equally.
Correspondence to: *s.dorbolo@uliege.be,**junzou@zju.edu.cn

ABSTRACT

The contact between droplets and granular materials is of practical importance for many processes, such as spraying cooling (to cool down the soil) and the wet dusting (to collect the grains). While the phenomenon is commonly known in nature and industry, our knowledge of the interaction between the water drop and hot grains is still very limited. Here, we experimentally investigated the drop behaviours released on a heated granular bed. Surprisingly, we found that the drops start digging the granular material as deep as 15 times the diameter of the droplet. Hot particles are absorbed into the drop and vaporise the liquid. The vapour production is so intense that the vapour is able to blow away the particles underneath the drop. The drop can then move downwards under the action of the gravity. In order to inspect this digging behaviour, two kinds of setups were designed: a 3D granular packing inside a cylinder and a quasi-2D packing inside a Hele-Shaw cell. The first allows the observation of the droplet with the heated material, while the second provides the direct observation from the side view to uncover the drop behaviour in the deep bed. One proposes a mechanism based on the Leidenfrost effect considering a rough surface that models the surface of the granular material. This model allows to explain why the droplet can dig on a range of temperatures between the boiling temperature of the cooling liquid and the Leidenfrost temperature relative to the granular material. In this range of temperatures, the cooling of the granular material is then rather efficient since the droplets vaporise deeply in the heart of the material.

When a liquid drop meets a hot solid, the heat transfer can be large enough to provoke the continuous vaporisation of the droplet. Under these conditions, a film of vapour separates the liquid and the solid; this is called the Leidenfrost effect[1–3]. The conditions that affect the temperature of transition towards the calefaction state depend on the nature of the liquid (mostly the temperature of transition and the latent heat), the nature of the solid (the thermal conductivity must be large enough to allow the rapid heat transfer to the droplet) and the geometrical configuration (the shape and the surface roughness of the solid). One can find a nearly complete panel of works that tackles the different contributions which allows to obtain reliable models to describe the shape of the droplet and the vaporisation rate. The prediction of the temperature of transition is still debated mainly because the surface roughness role is difficult to model within the actual theory. On the other hand, the temperature of transition corresponds to the liquid-vapour temperature transition of the droplet when the solid is substituted by a liquid, for example on a bath of hot oil[4]. The roughness of the liquid is indeed non sense. Nevertheless the thermal conductivity of liquids is low compared to metals. This lack of conductivity is compensated by the convective recirculation inside the liquid triggered by the cooling of the surface and the bulk induced by the droplet and by the vapour entrainment[5].

In the XIX century, after the work by Boutigny[6], the Leidenfrost effect was seen as a particular state of the matter that would allow precise manipulation of liquids to generate chemical reaction. This precursor principle was applied a decade ago by Elbahri[7,8]. Indeed, the droplet in Leidenfrost state can be seen as a chemical reactor without solid border avoiding the

Table 1 Characteristic diameters for the grains

Sample name	d_{10}	d_{50}	d_{90}	$d_{3,2}$	$d_{4,3}$
SiC-I	19	35	63	28	38
SiC-II	28	42	65	40	44
SiC-III	36	59	95	55	62

All values stated in μm.

d_k denotes the *k th* percentile for the particle size distribution.

The sizes $d_{3,2} = \sum_{i-1}^{n} d_i^3 / \sum_{i-1}^{n} d_i^2$ and $d_{4,3} = \sum_{i-1}^{n} d_i^4 / \sum_{i-1}^{n} d_i^3$ refer to surface-area-based mean diameter and volume-based mean diameter respectively. One use $d_{3,2}$ to characterize the typical radius r of the beads, i.e. $2r = d_{3,2} = d_g$.

nucleation on the border and the contamination. On the other hand, the Leidenfrost effect is a strong issue regarding cooling processes. When a surface is heated to extreme temperature, the cooling efficiency using water is drastically reduced by the formation of the vapour layer between the droplet and the solid to cool down. This effect was critical during the operation in Fukushima nuclear accident[9]. Actually, increasing the roughness of the surface is the only way to increase the Leidenfrost temperature transition.

Along the same line of ideas, one can question the ability of droplets to cool down a granular soil[10]. First, it is well known that after the passage of wildfires, the soils are hydrophobic and any droplet that impacts this soil is covered by thin dust particles[11]. As a consequence, the water streams without penetrating the soil. One expects that such a behaviour may occur during the fire extinction. On top of that, the granular materials are poor thermal conductors because the contact between the grains are numerous and characterised by a high thermal resistance. In a recent report concerning the thermal conductivity of steel beads, the effective thermal conductivity is found to decrease by a factor 100 compared to the bulk thermal conductivity of the steel[12, 13]. As far as the problem of the calefaction is concerned, granular materials are not supposed to be a good candidate to trigger the Leidenfrost transition (i) because the surface of a granular material is very rough typically the size of the grains, (ii) because the poor thermal conductivity does not guarantee that the heat can be transferred fast enough to sustain the intervening vapour film and (iii) because the grains can move under the action of the droplet and can even be trapped by the droplet as seen at room temperature[14–16] or at high temperature[10,17]. On the other hand, the direct contact (trapping) with the grains allows a rapid heat transfer to the droplet which could provoke a high rate of production of vapour. In this work, we present original experiments during which the droplet was gently dropped on a heated granular material. One observed that the droplet can self-bury into the granular material keeping its spherical shape during the digging process. The droplets is then able to reach depths up to 15 times its diameter. This is this surprising phenomenon that we will describe and explain.

Two experimental set-ups were dedicated to the exploration of the impact of a room temperature water drop onto a granular bed. The first one, named 3D, consisted in a thick cylinder filled with grains. The second, one named quasi-2D, consisted in a Hele-Shaw cell which one wall was made of sapphire in order to directly inspect the motion of the droplet inside the granular material.

We used grains made of silicon carbide (SiC) because of their high thermal conductivity $\lambda_{SiC} = 83.6$ W/m/K compared to sand $\lambda_{sand} \approx 0.15$ W/m/K. The grain size was analysed by a laser particle size analyser (Mastersizer 2000,Malvern Instruments). The particles possess irregular shapes and mono-modal size distributions (see Table 1). Since these grains are mostly non-spherical, we used surface-area-based mean diameters as the characteristic diameter, i.e. $d_g = d_{3,2}$= 28, 40 and 55 μm for three types of SiC powder respectively (see the definition of $d_{3,2}$ in the caption).

The 3D setup is depicted in Fig. 1a. A cylindrical vessel (about 30 mm of inner diameter for a height of 10 mm) made of aluminium was placed on a temperature controlled plate. After the thermalisation of the granular bed (that was checked using a

thermocouple), the droplets were released 10 mm above the surface of the granular material and filmed under an angle of about 45°. The droplet diameter $2R$ was 2.8 mm. Note that a temperature gradient existed and was measured between the very surface of the granular bed and under the surface (see Supplemental Information, sect. S1). The average temperature of the top of the bed T_s is chosen as the characteristic temperature here. One defines the superheat ΔT as the difference between the actual temperature T_s and the boiling point of the water $T^* = 100°C$.

As for the 2D setup , it consisted in a vertical Hele-Shaw cell which dimensions was $42 \times 45 \times 3$ mm (shown in Fig. 2a). This system allowed to observe the motion of the droplet and of the grains thanks to a transparent window made of sapphire (see Materials and Methods). The bed temperature T_b was tuned between 100°C and 450°C. One defines the superheat ΔT as the difference between the actual temperature T_b and the boiling point of the water $T^* = 100°C$.

Results

Drop on a hot granular packing

Let us first consider the 3D case. Compared to a droplet, with a radius $R = 1.4$ mm, gently released on a granular bed at room temperature (see Movie-S1), the interaction drop-grains on the heated granular bed is rather violent. The liquid is heated by direct contact with the hot particles and generates a strong vapour flow, which expels particles into the air forming a granular fountain (as shown in Fig. 1b,c (second image); see also the Movie-S2/S3). The particle ejection occurs when the temperature of the substrate T_s is larger than the boiling temperature of the water.

According to the temperature, one can identify two regimes characterized by the final pattern observed at the surface of the granular bed. The patterns are shown in the fourth images of the Fig.1b,c.

Regime I (Fig. 1b): For $100°C < T_s <\approx 165°C$, the droplet penetrates into the granular material and disappears under the fountain of grains. In this regime, the granular fountain mainly occurs along the edge of the droplet (also see the Movie-S2). This behaviour is similar to what is observed when the thickness of the layer of grains is of ther order of the droplet diameter[10]. At the end, namely when the droplet is completely evaporated, a circular chain of holes forms at the surface that corresponds to the perimeter of the drop as shown in Fig. 1b (the grain size $d_g = 55\,\mu$m and the bed temperature $T_s = 165\,°C$). One can gently remove the grains surrounding the fountain in order to observe an assembly of grains collected by the droplet. The situation is similar to what happens at room temperature (Fig. S4a), namely the drop captures particles and eventually form a collection of cohesive particles even after the complete vaporisation. In this regime, the particle collections is found in the shallow layer of the granular bed and is nearly spherical. The assembly is partly exposed to the air or is just covered by a few layers of particles.

Regime II (Fig. 1c): For $T_s > 165\,°C$, the contact of the droplet with the grains results in a very large fountain of grains. The ejection of particles leads to a crater that increases its size because of the avalanche effect and the collapse of the crater edge. The droplet penetrates the granular material and then disappears under the surface. The Figure 1c shows a large crater formation at $T_s = 300\,°C$ for the same grains as in Fig. 1b. Contrary to the regime I, the assembly of grains (cohesive after being wet) is found deep inside the granular bed (e.g. the particle collection was found at the bottom of the container with $T_s = 300\,°C$ and $d_g = 55\,\mu m$). However, the shape of the assembly is still spherical (see Movie-S4 and Supplemental Information, sect. S2). In both regimes, the obtained assembly is a sphere which diameter is very close to the diameter of the initial droplet.

The 3D granular bed experiments provide a global view of the interaction between drops and a high temperature granular bed. However, the experimental set-up is unable to provide a perspective of what happens inside the granular beds. To better understand the interaction between the droplet and the heated granular bed, quasi-2D experiments are necessary. The 2D setup has a limitation due to the presence of the sapphire window. Indeed, the bed temperature T_b must be set to a value higher than the Leidenfrost point (nearly 200 °C). Otherwise, the drop contacts the sapphire wall. As a consequence, only the regime II can be discussed using this device.

Visualisation in a quasi-2D container

In Fig. 2b (also see Movie-S6), the drop is shown while digging the granular material. The bed temperature was set to $T_b = 300\,^{\circ}\mathrm{C}$ and the grain size $d_g = 28\,\mu m$ (SiC-I). As the drop contacts the granular beds ($t = 0$), a small part of particles are absorbed into the drop. Meanwhile, the vaporisation of the liquid generates a strong vapour flow that expels upwards the particles initially located under the drop. The ability to remove the underlying particles implies the drop itself moving downwards: the droplet digs in the granular bed. The vapour flow entrains the particles out of the granular bed feeding the granular fountain. Actually, one observes that the granular material is fluidised from the top of the droplet to the surface. The fluidised region has cylindrical shape from the top of the droplet to about 10 mm below the initial surface of the granular bed. Above this limit, the granular crater develops. The drop digs at approximately a constant speed $v_0 \approx 4$ mm/s between $t = 0$ to $t = 10.4$ s and then stops suddenly at a depth that is about 14 times the radius of the droplet (also see Fig. 3a). On the other hand, the granular fountain keeps on expelling grains for another 7 s after the droplet stops digging. It is worth noting that, during the digging process, more and more particles are absorbed into the droplet. This leads to the formation of a particle collections, which is also found in the 3D granular bed experiments. The liquid drop seems to be saturated with particles at the moment that digging stops.

One can plot the position H ($H = 0$ corresponds to the surface) of the droplet as a function of time for different temperatures. The results are shown in Fig.3a. The last point of each curve corresponds to the end of the vaporisation of the droplet, i.e. when the fountain stops. One can decompose the dynamics into two regimes: a digging regime and a standing vaporisation regime. The digging regime includes two steps. First, the drop moves slowly to cross the air-granular material interface (this is the coldest part of the granular bed as explained in the supplemental material). As soon as the droplet is below the surface, namely H is of the order of the diameter D of the droplet, the digging speed v_d increases and remains constant (H is linear with time, see Fig. 2b, 3a). During the motion, particles are collected by the droplet. Finally, the droplet stops at a depth H_{max} until the water is completely evaporated (standing vaporisation regime). Related to these three steps, three time laps can be defined: τ_i, the time to cross the interface, τ_d, the duration of the deep digging process and finally, τ_s the duration of the static state. The sum of the three times is equal to the lifetime of the droplet $\tau = \tau_i + \tau_d + \tau_s$. Note that one may suspect that vaporisation is not certain to end after the time τ; we determined τ_s when there is no motion any longer around the 'droplet'. These times are reported as a function of the superheat ΔT in Fig. 3b. One observes that the total lifetime remains roughly constant about 19 s. The crossing of the interface takes more and more time when the temperature is increased. The digging time $(\tau_i + \tau_d)$ increase with ΔT and consequently τ_s decreases with increasing ΔT. The increase of digging time $(\tau_i + \tau_d)$ is, according to the observations, related to the decrease of the particle trapping rate when the temperature increases (See Supplemental Information, sect. S3).

The final depth H_{max} reached by the particle is governed by the average digging speed v_d and the duration of the digging $(\tau_i + \tau_d)$. The final depths and the digging speeds are presented as a function of the superheat ΔT in Fig. 3c. While $v_d(\Delta T)$ decreases with the temperature, the maximum depth reached by the droplet presents a maximum at $\Delta T = 200\,^{\circ}\mathrm{C}$.

Discussion

Origin of the drop digging

The proposed mechanism is obviously related to the Leidenfrost process. Due to the proximity of the droplet to the hot bed of grains, under the action of the weight of the droplet F_w, water vapour is generated and released between the droplet and the hot surface. If the substrate were a solid, the created vapour feeds a thin vapour film. The thickness h of the film depends on the heat transfer from the substrate to the droplet and on the size of the droplet. When the heat transfer is sufficient, the squeezing of the vapour generates a vertical force due to lubrication that can be sufficient to lift the droplet. On a granular bed, the vapour generated by the vaporisation of the water can reach a sufficient speed v_v to eject the grains just under the droplet. The granular bed is then locally fluidised provoking the droplet to move downwards in the bed: the droplet digs. Instead of having a thin vapour film, the droplet sits on layer of fluidized granular bed which thickness depends on the heat transfer and on the geometry of the droplet. The digging speed v_d and the trapping rate are certainly related to this mechanism. A sketch of the situation is

proposed in Fig.2c.

To be convinced about the relationship between the gas production and the digging process, one has estimated the mass m_1 of vapour produced during the digging stage. That corresponds to the volume of water that has been replaced by grains. Assuming that the digging process stops when the droplet is full of grains, the evaporated mass can be estimated by $m_1 = \rho_l(\pi D^3/6 - (1-\phi)V_{ball})$, where ρ_l is the density of the liquid, $\phi = 0.64$ is the volume fraction of the grains (3D hexagonal compact) and V_{ball} is the volume of the granular ball (see Supplemental Information, sect. S3). If one reports the digging speed v_d as a function of the average vapour production $Q_{exp} = m_1/(\tau_i + \tau_d)$, one obtains the graphics of the Fig. 4a. One can see that whatever the grain size and for all the considered temperatures, the data collapses on one empirical master curve which shows that $v_d \propto (m_1/(\tau_i + \tau_d))^{1/3} - \alpha$,where α is a constant.

Having estimated the quantity of vapour generated in average, one can estimate the speed of the vapour by substituting the vapour flow rate Q by Q_{exp} in the following relation

$$Q = 2\pi R \rho_v h v_v \tag{1}$$

where ρ_v is the density of the vapour. Because the film is thin compared to the radius of the droplet, the lubrication hypothesis applies and the vapour exerts a shear stress τ_v on the grains proportional to $\mu \frac{v_v}{h}$ where μ is the dynamical viscosity of the vapour. One assumes that the transport rate of the grains Q_g is proportional to the effective shear stress that $(\tau_v - \tau_0)$[18,19], where τ_0 is the threshold of the shear stress requiring for grain transportation. The digging velocity of the drop v_d is linear to the transport rate of the underlying grains Q_g and one obtains that $v_d \propto Q_g$, and as a consequence, one finds a relation between the speed of the particles and the average vapour production rate, namely $v_d \propto (\frac{Q}{h^2} - \alpha)$. The vapour is propelled out of the droplet bottom under the pressure exerted by the droplet. One can estimate the vapour speed using the scaling from the lubrication theory

$$\frac{\Delta P}{\ell} = \mu \frac{v_v}{h^2} \tag{2}$$

where ΔP is the pressure difference between the South pole of the droplet and the equator and ℓ the distance the vapour has to move to escape, here $\ell \approx \pi R$. The pressure exerted by the droplet is due to the weight of the droplet but one could imagine that it should be corrected by the upwards entrainment by the grains (a vertical drag) or by a term of buoyancy that is to be taken into account in fluidised granular bed[20]. One assumes that this pressure is constant. Substituting the expression of the vapour speed from Eq.(1) into the equation of the lubrication Eq.(2), one obtains a relation between the vapour production rate and the vapour film thickness, that is $h \propto Q^{1/3}$. So, the expression of the digging speed becomes $v_d \propto (Q^{1/3} - \alpha)$ that was found experimentally.

Estimation of the digging speed

One has to explain the behaviour of the digging speed as a function of the temperature. Indeed, according to the measurement, the digging speed v_d decreases when the temperature is increased while the digging duration $(\tau_i + \tau_d)$ increases with the temperature. These two behaviours explain the observation of an optimal depth H_{opt}. Regarding the scalings developed in the previous paragraph, v_d decreases when the vapour production rate is decreased. This also means that the vapour production rate decreases when the temperature is increased. This later statement looks like a paradox.

The explain this paradox, one has to make a parallel with the situation of the droplet released on very rough and hot surface. Such a study has been performed by Kim[21] and was confirmed by measurements in high gravity environment[22]. Kim observed the evolution of the lifetime of droplet as a function of the temperature of a substrate which roughness was changed. When the substrate is smooth and the temperature of the substrate is close but lower than Leidenfrost temperature transition, the droplet evaporates very rapidly (a few seconds) because the droplet is sessile and the heat transfer is fast. Above the Leidenfrost temperature, the lifetime is as large as 100 times the lifetime below the transition because the vapour film decreases the heat transfer towards the droplet. On the other hand, when the surface is very rough, the transition to the Leidenfrost state is not

sharp but the lifetime continuously increases between the boiling temperature of the water and the Leidenfrost temperature. In this case, the increase of temperature means a decrease of heat transfer. One can imagine that such a mechanism holds also in the case of the heated granular material as the surface, made of grains, is intrinsically rough. To account of the evolution of the heat transfer with the increase of the temperature, the following mechanism is proposed.

In the classical Leidenfrost, one considers the heat transfer through the vapour film, one finds for the vapour production rate

$$Q = \frac{\kappa_v}{\mathscr{L}} \frac{S}{h} \Delta T \tag{3}$$

where κ_v is the thermal conductivity of the vapour (0.04 W/m/K), $\mathscr{L}$ is the latent heat to transform the water into vapour and S the surface of exchange, here one consider half the surface of the droplet $S = 2\pi R^2$. Combined with the equation of conservation Eq.(1) and the equation of lubrication Eq.(2), one finds a relation between the superheat and the vapour thickness, namely $h \propto \Delta T^{1/3}$. The hotter the substrate is, the thicker the film is. A more precise calculation can be found in ref.[5]. If the thickness h of the vapour film is smaller than the roughness of the substrate, here typically the diameter $2r$ of a grain, the droplet touches the grains. That means that the heat transfer also occurs directly from the grains to the droplet. Indeed, the thermal conductivity of the bulk SiC is very large compared to the vapour, i.e. $\kappa_{b,SiC}$=350 W/m/K. Even if the thermal conductivity of the granular material κ_{SiC} should be much lower (at least a factor 10)[23], this means that the thermal conductivity should be a function of the superheat.

Based on that mechanism, we propose a simple model that allows to explain the decrease of the vapour production rate and, consequently, the decrease of the digging speed when the temperature of the granular bed is increased. The principle is to consider the interaction between the droplet and a rough surface made of sphere. When the temperature is too low, the vapour gap generated by Leidenfrost effect is not sufficient to lift the droplet over the default of the surface. In consequence, the droplet touches the grains and more energy can be transported towards the droplet inducing an increase of the vapour production. When the temperature is increased, the vapour gap increases. Less and less grains are touched; the vapour production rate decreases when the temperature increases. As less and less grains are touched when the temperature increases, the trapping probability of grains inside the droplet decreases. Consequently, the digging time is also increased when the temperature is increased.

Here is the description of the algorithm. First, we compute the thickness h_c within the classical Leidenfrost scheme, namely as if the substrate were smooth using Eq.(1), Eq.(2) and Eq.(3). Then, we evaluate the effective thermal conductivity as following. One considers that the surface of the granular bed is made of a monolayer of half-spheres with a radius r_{rug} that modeled the rugosity of the surface. The altitude zero being the equator of the half-spheres, we cut half-spheres with an horizontal plane at an altitude corresponding to the thickness of the vapour layer in the framework of the Eq.(3), i.e. h_c. This plane intersects the spheres and we can evaluate the surface fraction of the plane occupied by the spheres. The radius of the intercepted circle $r^\star$ given by $r^\star = \sqrt{r_{rug}^2 - h_c^2}$, the surface fraction SF is simply given by $SF = \pi\phi r^{\star 2}/(2\sqrt{3}r_{rug}^2)$, where ϕ is the surface fraction of the monolayer of spheres (ideally $\phi = 0.84$ in the 2D hexagonal compact configuration). Using a similar scheme as to describe the thermal conductivity of a granular material[23], the effective thermal conductivity k_{eff} is then found to be

$$k_{eff} = SF\,\kappa_{SiC} + (1 - SF)\,\kappa_v \tag{4}$$

Here one considers that the thermal conductivity of the granular material κ_{SiC}. A study demonstrated that the thermal conductivity may decrease of a factor 10 when the material is in grains[24] but it should be even lower in this case as the granular material is partially fluidised by the vapour. Then the vapour production rate is re-evaluated replacing κ_v by κ_{eff}. The speed of the gas is then deduced using the equation of conservation Eq.(1) and then the shear force $F_s = \mu v_g/(h_c - r)\pi r^2$; the radius r is subtracted from the total height of the vapour film. Moreover the shear force must be sufficient to lift the weight of one grain.

As a consequence, the speed of the grains v_g follows as

$$v_g = \sqrt{\pi R(F_s - m_g)/m_g} \tag{5}$$

as the force acts on the grains until the grains can escape from below the droplet. The digging speed is simply given by

$$v_d = \frac{r}{R} v_g \tag{6}$$

The value of r_{rug} was adjusted such as the speed of the grains cancels at $\Delta T \approx 400$ K; that correspond to $r_{rug} = 72$ μm. In other words, at $\Delta T \approx 400$, the droplet does not touch the grains any more at this temperature and the shear force does not allow any transportation of grains. The parameter of ϕ was kept equal to 0.84 (the 2D packing fraction). Finally, the only adjustable parameter was the thermal conductivity of the granular material κ_{SiC}. The result is reported in Fig.3c; this is the blue curve. A rather good agreement is found for $\kappa_{SiC} = 0.7$ W/m/K using this simple model. This is much lower than the value of the bulk. The model is also able to predicted lifetime as a function of the superheat. The lifetime is reported in the inset of Fig.3c. The order of magnitude is correctly found but this cannot be compared to the digging duration extracted from the experiments and reported in Fig. (3b). Indeed, the presented simple model does not take into account the trapping process and the influence of both the sapphire window and of the back of the Hele-Shaw cell. One also expects that some upwards forces should be exerted on the droplet due to the flow of grains. Finally, one could think about a drag force or about some buoyancy similar to the fluid hydrostatic force[20].

Regarding the model, we varied the granular material thermal conductivity κ_{SiC} and the roughness size r_{rug} to observe their effects on the digging speed and the lifetime. The results for the Fig.4b. The blue continuous curve decorated with bullet is the reference case: $\kappa_{SiC} = 0.7$ W/m/K and r_{rug} =70 μm. The variations of r_{rug} and of κ_{SiC} are presented as continuous and dashed curves respectively. If one changes the value of r_{rug}, one can see that the digging speed goes to zero for larger superheat ΔT when r_{rug} is increased. Indeed, the thickness of the vapour layer has to be thicker in order to escape to the roughness. The squares and the triangles that decorate the continuous curves correspond to r_{rug} equal to 60 and 80 μm respectively (in both case, κ_{SiC} is kept constant at 0.7 W/m/K). On the other hand, the lifetime (see the inset, same legend) increases when the roughness is decreased. Both behaviours, on v_d and on the lifetime, show that the thermal transfer increases with the roughness. Ones also varied the thermal conductivity of the granular material. The dashed curved decorated with squares and triangles correspond to $\kappa_{SiC} = 0.35$ and 1.4 W/m/K respectively, the roughness $r_{rug} = 70$ μm in both cases. The decrease of the thermal conductivity has the effect to decrease the digging speed and to increase the lifetime.

Conclusion

We report the behaviour of droplet released on a deep granular bed which temperature is far above the boiling temperature of the liquid the droplet is made of. One observed that the droplet digs in the granular bed with a constant speed and that the speed depends non-linearly on the temperature. The visualisation using a Hele-shaw cell allowed to extract the precise trajectory of the droplet and to deduce the mechanism for the digging. For temperature just above the boiling temperature, the droplet touches the grains producing a large amount of vapour that locally fluidises the granular bed just below the droplet. The droplet digs fast but not for a long time because grains are trapped during the process. For larger temperatures, the vapour gas layer becomes thicker as more gas is produced. As a consequence, less and less grains are touched by the droplet. The heat transfer is therefore also reduced. On the whole, the digging speed decreases with the temperature, less grains are trapped and the digging duration increases. When the temperature is too large, one reaches a nearly classical Leidenfrost state, namely the droplet levitates above the granular bed. As the digging speed decreases while the digging duration decreases when the temperature increases, it is only natural to find an optimum depth reached by the droplet. A simple model was reported to rationalise the experiments. The model accounts for the decrease of heat transfer when the temperature of the substrate is increased.

The cooling of an assembly of grains by a liquid presents different dynamics according to the temperature difference

between the cooling liquid and the grains. We showed that the range of temperature above the boiling temperature of the liquid is particularly favourable for a efficient cooling of the grains because the droplets penetrate deeply in the granular material cooling the material at its heart.

Materials and Methods

The experimental setups used in this work are shown in Fig. 1a and 2a. For all of the experiments and data presented in the main text, we use deionised water and commercial silicon carbide(SiC) abrasive ($\rho_g = 3.2\,g/cm^3$) as the granular material. A syringe with a needle was used to generate uniform drops, which had a diameter of $D = 2.8\,mm$. Three kinds of abrasive, which have a particle diameter d_g = 28, 40, and 55 μm respectively, were used in the experiments. The particles possessed irregular shapes and polydispersity. The contact angle of the solid particles with the water was estimated as 70-90°. The superhydropphobic SiC particles were made by coating a layer of silica nanoparticles on the normal particles. A commercial agent (Glaco mirror coat 'zero', Soft 99 Co.) was used for the particle coating. The drop behaviours were recorded by a high-speed camera (Phantom V2512) at 50-2000 fps (frame per second).

Setup for the 3D Granular beds experiments

The 3D experiments were based on a cylindrical granular packing placed on a thermostatic heater. To obtain the granular packing, particles were poured into a hopper and fall freely to fill a cylindrical aluminum container (depth = 10 mm, inner diameter = 31 mm, wall thickness = 2 mm). The granular packing in the container was scraped by a microscope slide to ensure a uniform, level surface. The packing fraction was $\phi = 0.42 \pm 0.02$. The granular beds were then heated to a target temperature by the thermostatic heater for more than 30 minutes. A set of surface temperature (T_s = 25 - 300 °C) could be achieved when the thermostatic heater was controlled in 25 - 450 °C (see Supplemental Information, sect. S1).

Setup for the quasi-2D Granular beds experiments

The quasi-2D granular beds were based on a Hele-Shaw cell, which had a size of $42 \times 45 \times 3$ mm. The cell was backed on a aluminum block which has 4 heating tubes inside. The aluminum block worked as a thermostatic heater could adjust the bed temperature T_b from 100 to 450 °C. The front side of the cell was covered by a sapphire allowing a side view of the digging process. The cell was firstly filled by particles. Then an electromagnet was used to tap the aluminum container which consequently adjusted the packing fraction of the granular beds . The packing fraction was $\phi = 0.39 \pm 0.01$ in present work.

Acknowledgements

This research has been supported the National Natural Science Foundation of China (grant no.51875507). SD thanks Zhejiang University for the visitor collaboration grant. SD also thanks F.R.S.-FNRS for financial support as Senior Research Associate.

References

1. Leidenfrost, J. *De aquae communis nonnullis qualitatibus tractatus* (1756).
2. Biance, A. L., Clanet, C. & Quéré, D. Leidenfrost dynamics. *Phys. Fluids* **15**, 1632–1637 (2003).
3. Quéré, D. Leidenfrost dynamics. *Annu. Rev. Fluid Mech.* **45**, 197–215 (2012).
4. Maquet, L. *et al.* Leidenfrost drops on a heated liquid pool. *Phys. Rev. Fluids* **1**, 053902 (2016).
5. Sobac, B. *et al.* Self-induced flows enhance the levitation of leidenfrost drops on liquid baths. *Phys. Rev. Fluids* **5**, 062701 (2020).
6. Boutigny, P. *Nouvelle branche de la physique ou Étude de l'état sphéroïdal.* (1847).
7. Elbhari, M., Paretkar, D., Hirmas, K., Jebril, S. & Adelung, R. Anti-lotus effect for nanostructuring at the leidenfrost temperature. *Adv. Mater.* **19**, 1262 (2007).

8. Abdelaziz, R. *et al.* Green chemistry and nanofabrication in a levitated leidenfrost drop. *Nat. Commun.* **4**, 2013 (2007).

9. min Kwon, H., Bird, J. & Varanasi, K. K. Increasing leidenfrost piont using micro-nano hierarchical surface structures. *Appl. Phys. Lett.* **103**, 201601 (2013).

10. Liu, D., Nguyen, N., Nguyen, N. V. & Tran, T. Sailing droplets in superheated granular layer. *Phys. Rev. Lett.* **125**, 168002 (2020).

11. McHale, G., Newton, M. & Shirtcliffe, N. Water-repellent soil and its relationship to granularity, surface roughness and hydrophobicity: a materials science view. *Eur. J. Soil Sci.* **56**, 445–452 (2005).

12. Polamuri, D. & Thamida, S. Experimental determination of effective thermal conductivity of granular material by using a cylindrical heat exchanger. *Int. J. Heat Mass Transf.* **81**, 767–773 (2015).

13. Govender, N. *et al.* The effect of particle shape on the packed bed effective thermal conductivity based on dem with polyhedral particles on the gpu. *Chem. Eng. Sci.* **219**, 115584 (2020).

14. Delon, G., Terwagne, D., Dorbolo, S., Vandewalle, N. & Caps, H. Impact of liquid droplets on granular media. *Phys. Rev. E* **84**, 046320 (2011).

15. Zhao, S., de Jong, R. & van der Meer, D. Raindrop impact on sand: a dynamic explanation of crater morphologies. *Soft Matter* **11**, 6562–6568 (2015).

16. Zhao, S., de Jong, R. & van der Meer, D. Liquid-grain mixing suppresses droplet spreading and splashing during impact. *Phys. Rev. Lett.* **118**, 054502 (2017).

17. Maquet, L., Colinet, P. & Dorbolo, S. Organization of microbeads in leidenfrost drops. *Soft Matter* **10**, 4061–4066 (2014).

18. Martin, R. L. & Kok, J. F. Wind-invariant saltation heights imply linear scaling ofaeolian saltation flux with shear stress. *Sci. Adv.* **3**, e1602569 (2017).

19. Phtz, T. & Durn, O. Unification of aeolian and fluvial sediment transport rate from granular physics. *Phys. Rev. Lett.* **124**, 168001 (2020).

20. Huerta, D., Sosa, V., Vargas, M. & Ruiz-Suárez, J. Archimedes' principle in fluidized granular systems. *Phys. Rev. E* **72**, 031307 (2005).

21. Kim, H., Truong, B., Buongiorno, J. & Hu, L. On the effect of surface roughness height, wettability, and nanoporosity on leidenfrost phenomena. *Appl. Phys. Lett.* **98**, 083121 (2011).

22. Maquet, L. *et al.* Leidenfrost drops: Effect of gravity. *Europhys. Lett.* **110**, 24001 (2015).

23. Tavman, I. Effective thermal conductivity of granular porous materials. *Int. Commun. Heat Mass Transf.* **23**, 169–176 (1996).

24. Huetter, E., Koemle, N., Kargl, G. & Kaufmann, E. Determination of the effective thermal conductivity of granular materials under varying pressure conditions. *J. Geophys. Res.* **113**, e12004 (2008).

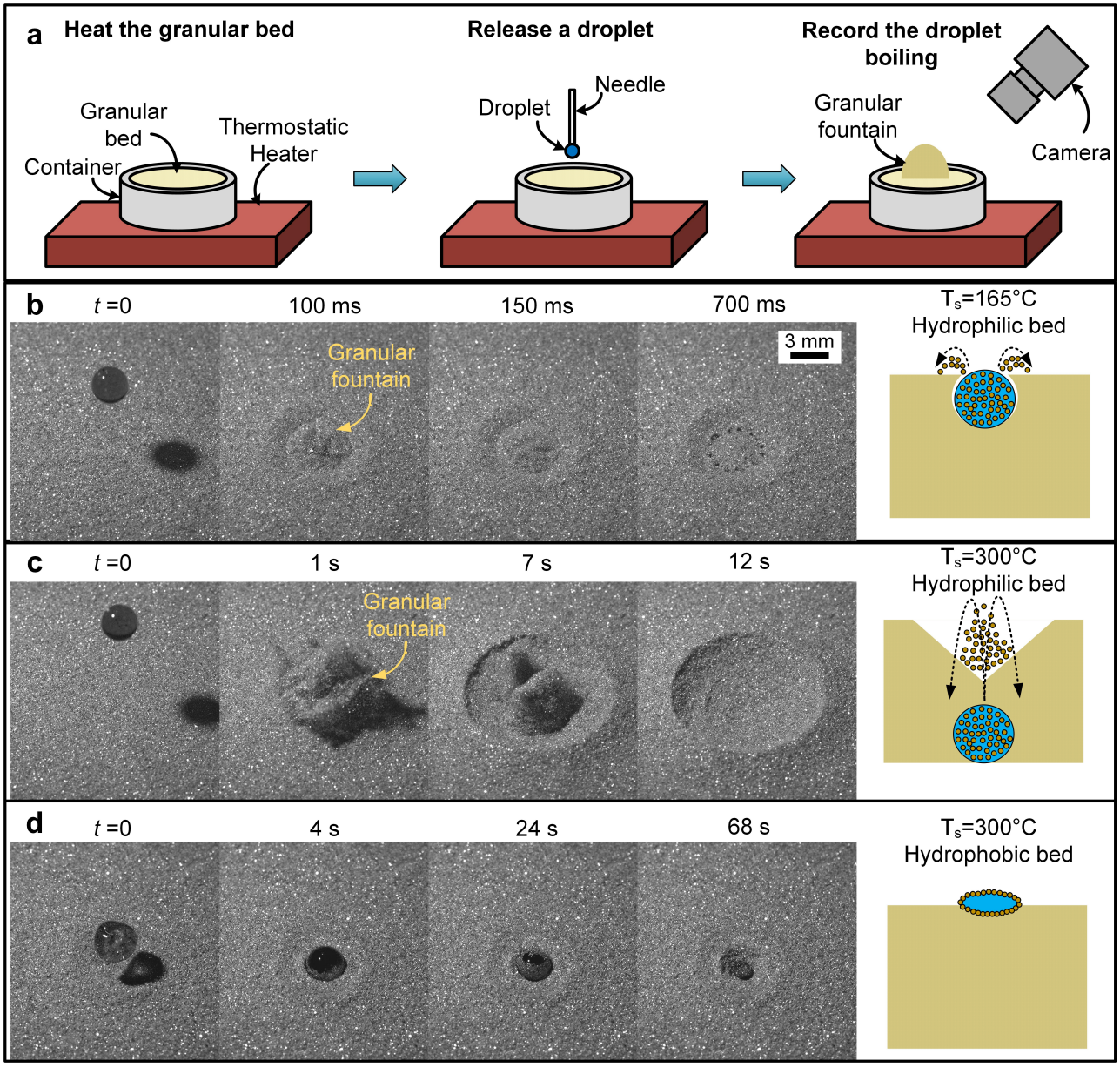

Figure 1. **(a)** 3D setup: A cylindrical container was filled with SiC grains. The temperature was set using a thermostatic plate. The penetration of the water droplet was recorded by a high speed camera under an angle of 45°. **(b)** Drop released on a hydrophilic granular bed at $T_s = 165°C$ (Regime I). Sand boiling effect is visible as a granular fountain starts nearly instantaneously after the contact between the droplet and the grains. The droplet boils near the interface of the bed. When the granular fountain settles down (nearly 700 ms), small holes remain at the surface. They are found along the initial perimeter of the droplet and are regularly spaced. (see the fourth image in **b** and Movie-S2). **(c)** The heated bed of grains ($d_g = 55\ \mu$m) was heated up to a temperature $T_s = 300°C$. the water is completely vaporised after 12s. After the complete vaporisation of the droplet, the droplet expels a large amount of grains far from the impact. A crater is then obtained after the full vaporisation of the droplet (see Movie-S3). In both case (b) and (c), a spherical assembly of grains were found under the surface. **(d)** For comparison, the same grains were coated with hydrophobic molecules ($T_s = 300°C$). Because of the treatment, the water droplet cannot penetrate anymore under the surface of the granular material (see Movie-S5).

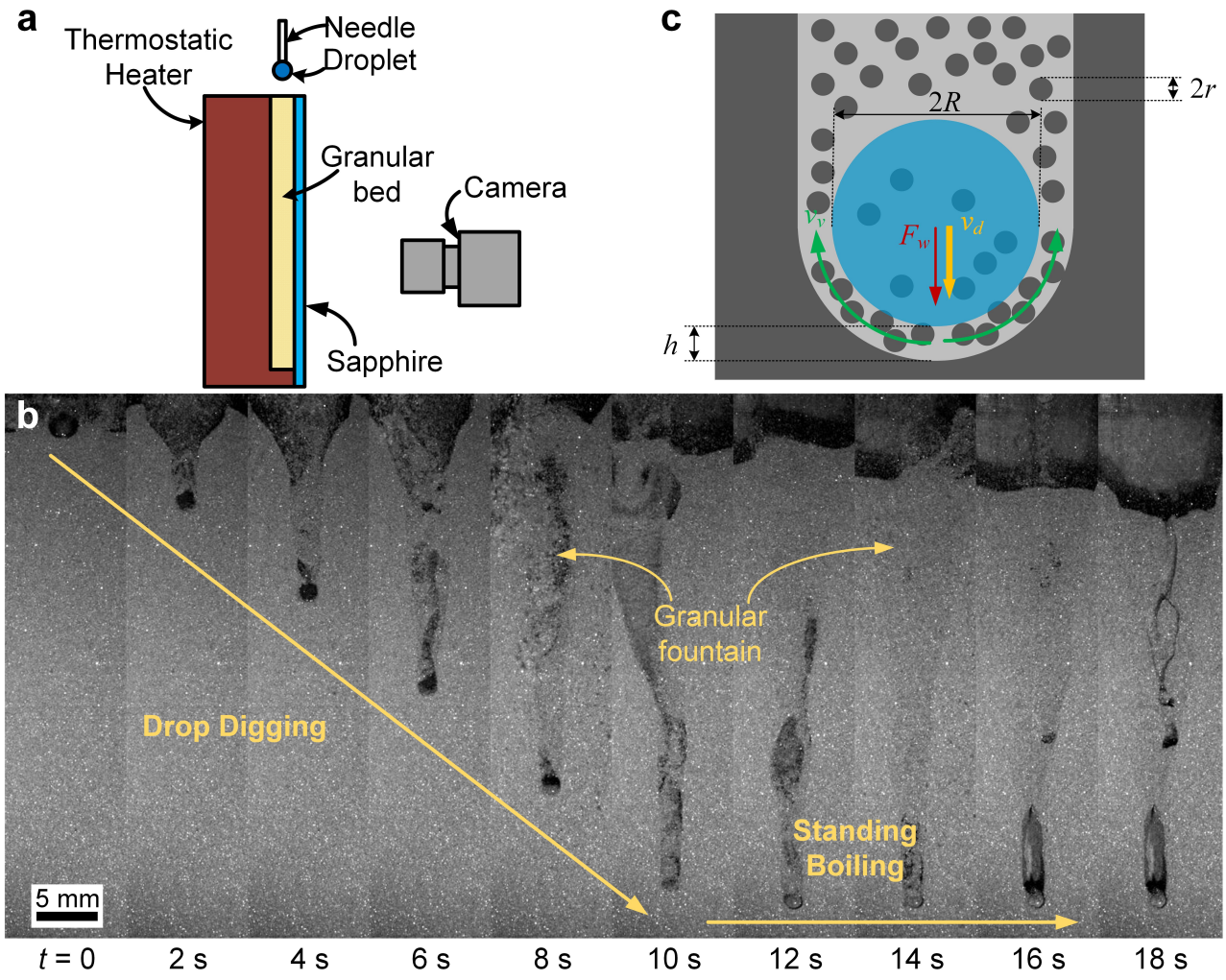

Figure 2. **(a)** 2D setup: a Hele-shaw cell was constructed and filled with SiC grains. One of the vertical wall was heated and kept at a constant temperature while the opposite wall was made of sapphire in order to record the motion of the droplet below the surface using a high speed camera. **(b)** Typical 2D view side of the digging process (also see Movie-S6). The temperature of the granular bed is T_b=300°C. The pictures are timely separated by 2 s. The maximum digging depth $H_{max} = 39.0$ mm. One can easily see that the droplet moved at a constant speed until $t = 10$ s. Above the droplet, the granular bed was fluidised along a vertical cylinder which diameter corresponds to the diameter of the droplet until 10 mm from the surface. Then the fluidised granular part forms a funnel shape at the surface, i.e. the crater. The crater diameter was observed to increase with time. For $t > 10$ s, the droplet did not go downwards anymore. The grains remained fluidised until the complete vaporisation of the water. **(c)** Sketch of the digging droplet. The digging droplet is modeled as a droplet surrounded by an air-granular mixture layer that are ejected under the action of the produced vapour.

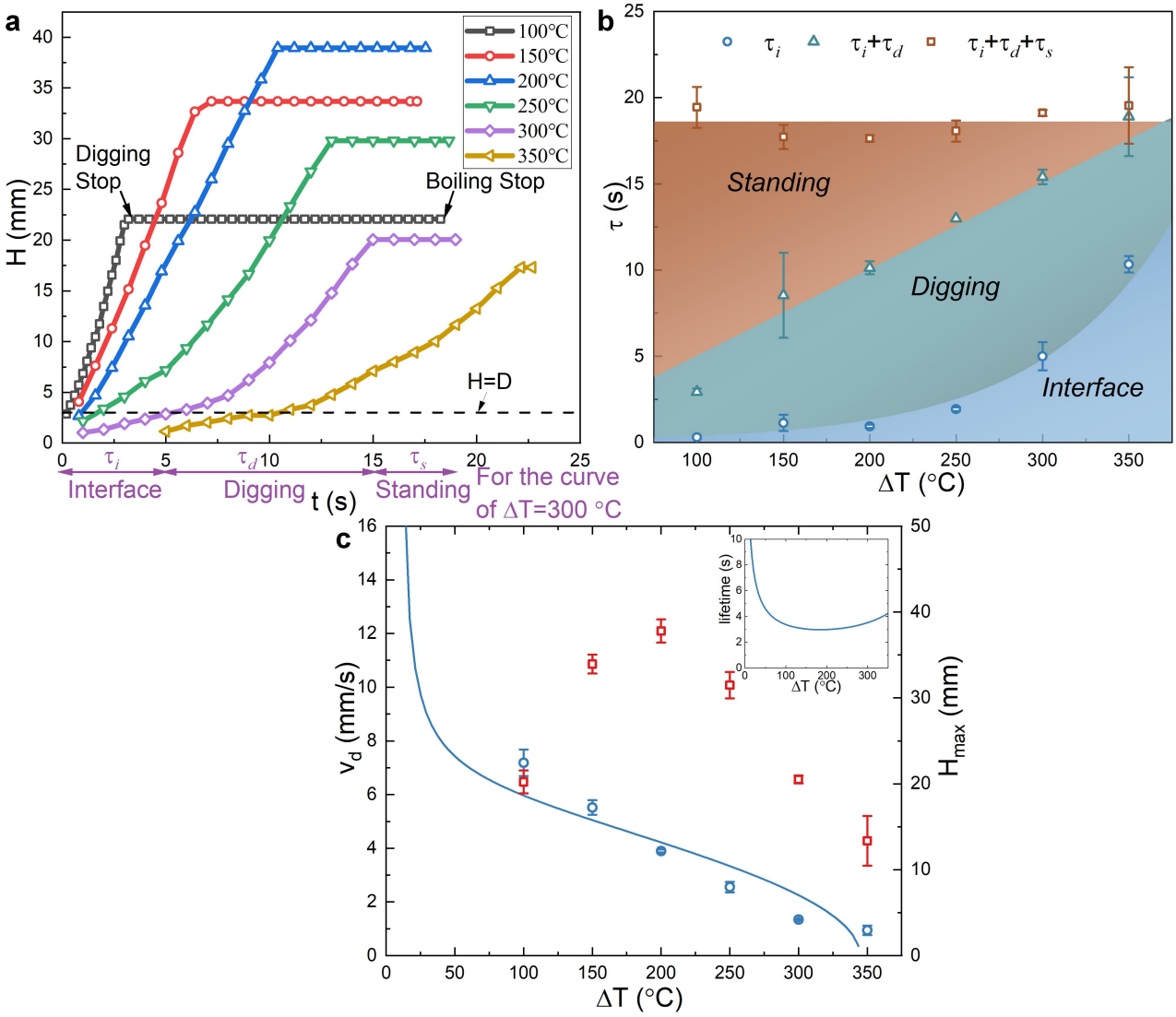

Figure 3. **(a)** Height reached by the droplet as a function of time for different temperatures between 200 and 450°C (see Legend). Three steps can be identified: the time to cross the interface τ_i, the deep digging process during the time τ_d and the stand-by state during τ_s. In red, the different step durations are represented for the case $T_b = 400$°C. **(b)** Distribution of the duration of the different steps (τ_i, τ_d and τ_s are the black squares, the red circles and the blue triangles respectively) during the digging process as a function of the superheat ΔT. The total duration of the process remains constant. The time to cross the interface increases with the superheat. On the other hand, since the standing time linearly increases with ΔT, the digging duration is maximum when $\Delta T = 250°$ C. **(c)** The maximum depth reached by the droplet is presented as a function of the temperature (red squares). A maximum depth is reached for ΔT =300 °C. The speed during the digging process is also presented as a function the granular bed superheat (blue bullets). The speed keeps on decreasing with the temperature. The curve correspond to the model presented in the discussion section for r_{rug} =70 μm, κ_{SiC} =0.70 W/m/K.

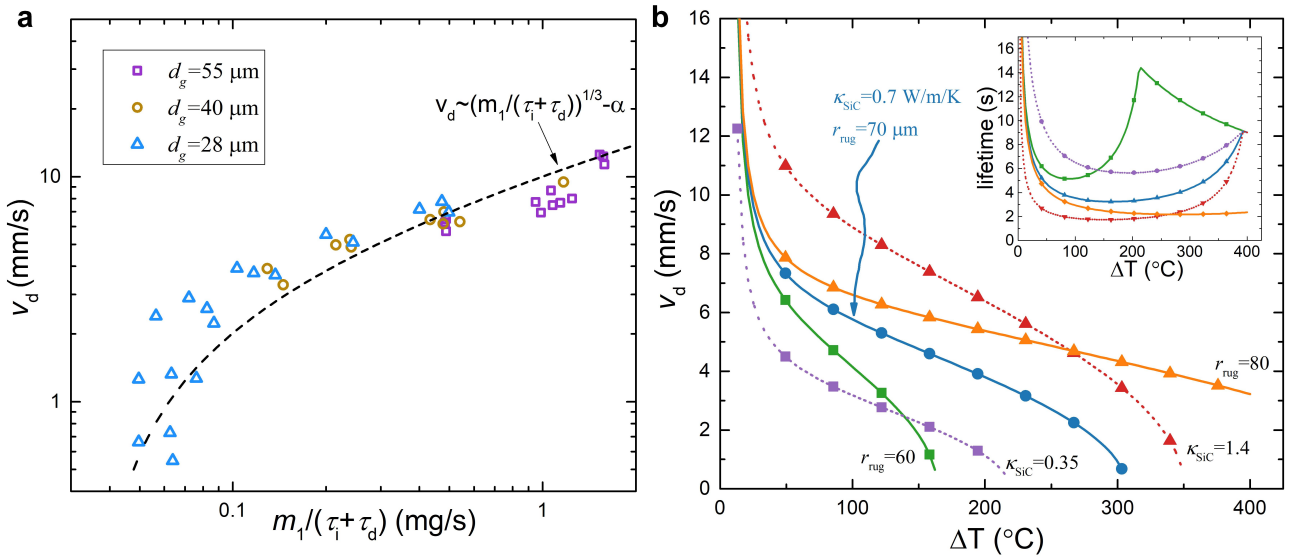

Figure 4. **(a)** Digging speed as a function of the experimental vapour production namely $m_1/(\tau_i + \tau_d)$. The dashed curve correspond to a fit by a power law 1/3. **(b)** Digging speed and vaporisation lifetime (inset) determined by the model as a function of the superheat ΔT. The best fit case, $r_{rug} = 70$ μm and κ_{SiC}=0.7 W/m/K (continuous blue curve decorated with bullets) is compared to different values of r_{rug} and κ_{SiC}. The continuous curves correspond to r_{rug}=60 and 80 μm (green squares and orange triangles respectively) κ_{SiC}=0.7 W/m/K. The dashed curves correspond to κ_{SiC}=0.35 and 1.4 W/m/K (purple squares and red triangles respectively) r_{rug}=70 μm.

Figures

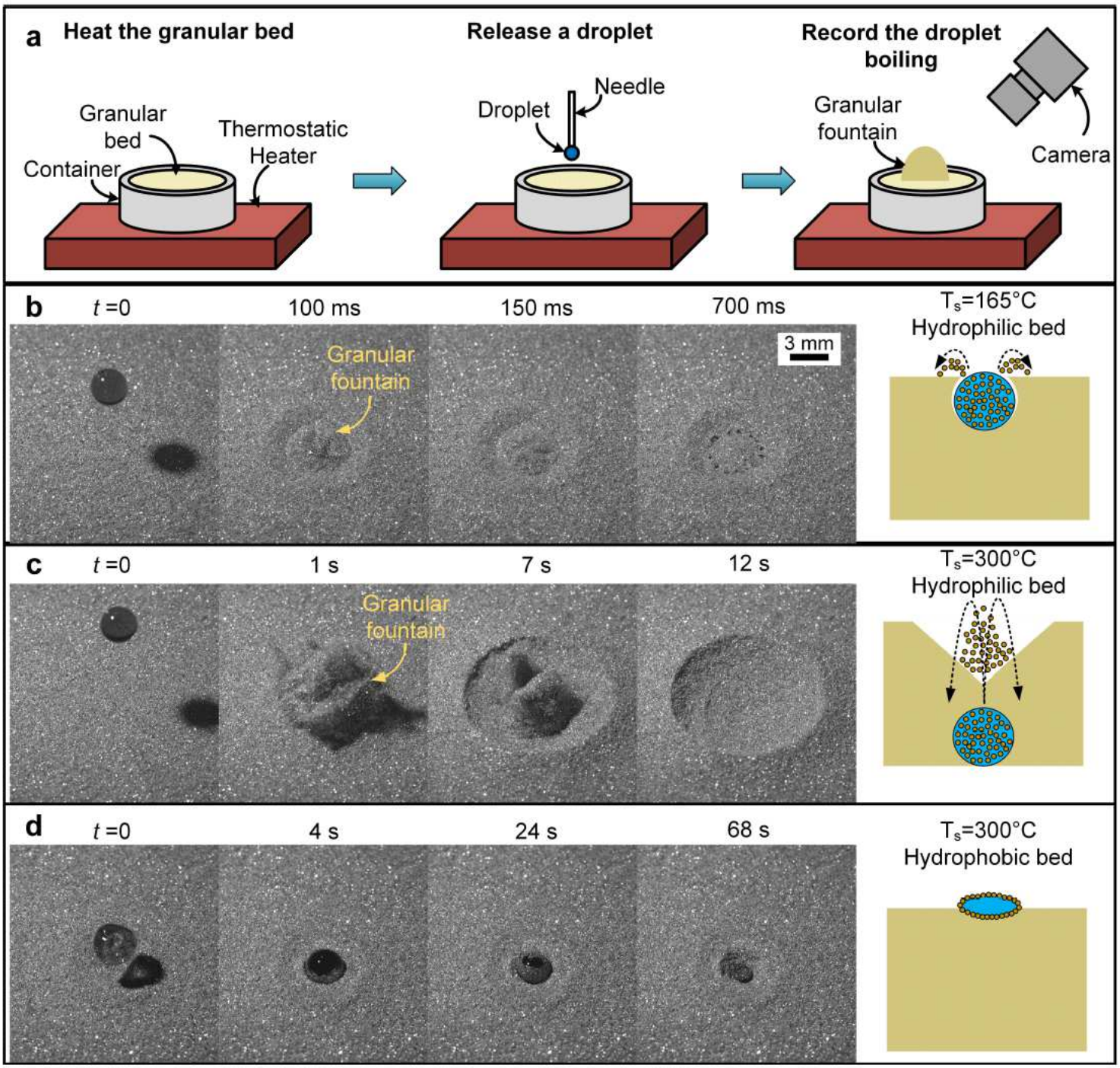

Figure 1

(a) 3D setup: A cylindrical container was filled with SiC grains. The temperature was set using a thermostatic plate. The penetration of the water droplet was recorded by a high speed camera under an angle of 45°. (b) Drop released on a hydrophilic granular bed at Ts = 165°C (Regime I). Sand boiling effect is visible as a granular fountain starts nearly instantaneously after the contact between the droplet and the grains. The droplet boils near the interface of the bed. When the granular fountain settles down (nearly 700 ms), small holes remain at the surface. They are found along the initial perimeter of the

droplet and are regularly spaced. (see the fourth image in b and Movie-S2). (c) The heated bed of grains (dg = 55 µm) was heated up to a temperature Ts = 300°C. the water is completely vaporised after 12s. After the complete vaporisation of the droplet, the droplet expels a large amount of grains far from the impact. A crater is then obtained after the full vaporisation of the droplet (see Movie-S3). In both case (b) and (c), a spherical assembly of grains were found under the surface. (d) For comparison, the same grains were coated with hydrophobic molecules (Ts = 300°C). Because of the treatment, the water droplet cannot penetrate anymore under the surface of the granular material (see Movie-S5).

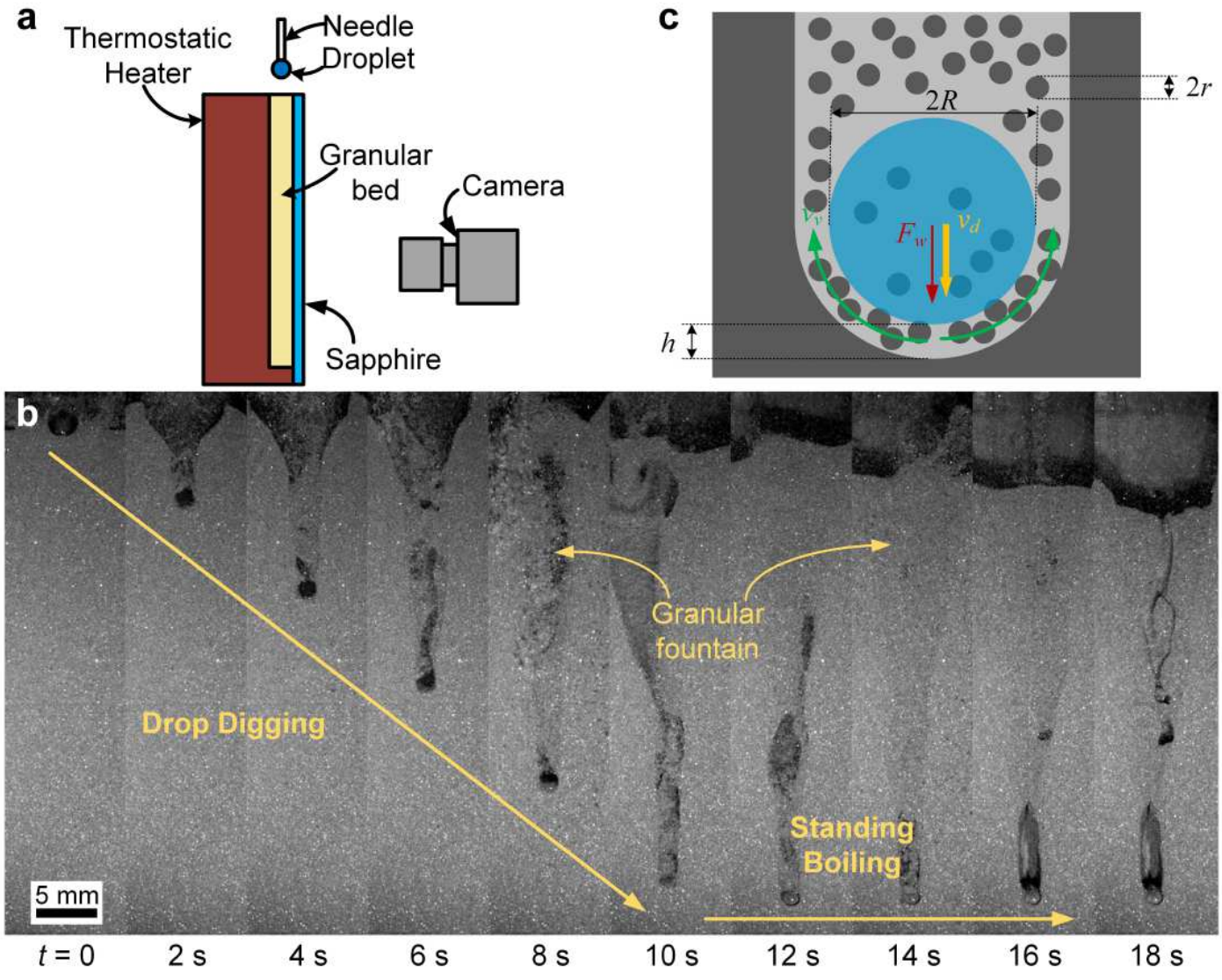

Figure 2

(a) 2D setup: a Hele-shaw cell was constructed and filled with SiC grains. One of the vertical wall was heated and kept at a constant temperature while the opposite wall was made of sapphire in order to record the motion of the droplet below the surface using a high speed camera. (b) Typical 2D view side of the digging process (also see Movie-S6). The temperature of the granular bed is Tb=300°C. The pictures are timely separated by 2 s. The maximum digging depth Hmax = 39.0 mm. One can easily see that the droplet moved at a constant speed until t =10 s. Above the droplet, the granular bed was fluidised along a

vertical cylinder which diameter corresponds to the diameter of the droplet until 10 mm from the surface. Then the fluidised granular part forms a funnel shape at the surface, i.e. the crater. The crater diameter was observed to increase with time. For t > 10 s, the droplet did not go downwards anymore. The grains remained fluidised until the complete vaporisation of the water. (c) Sketch of the digging droplet. The digging droplet is modeled as a droplet surrounded by an air-granular mixture layer that are ejected under the action of the produced vapour.

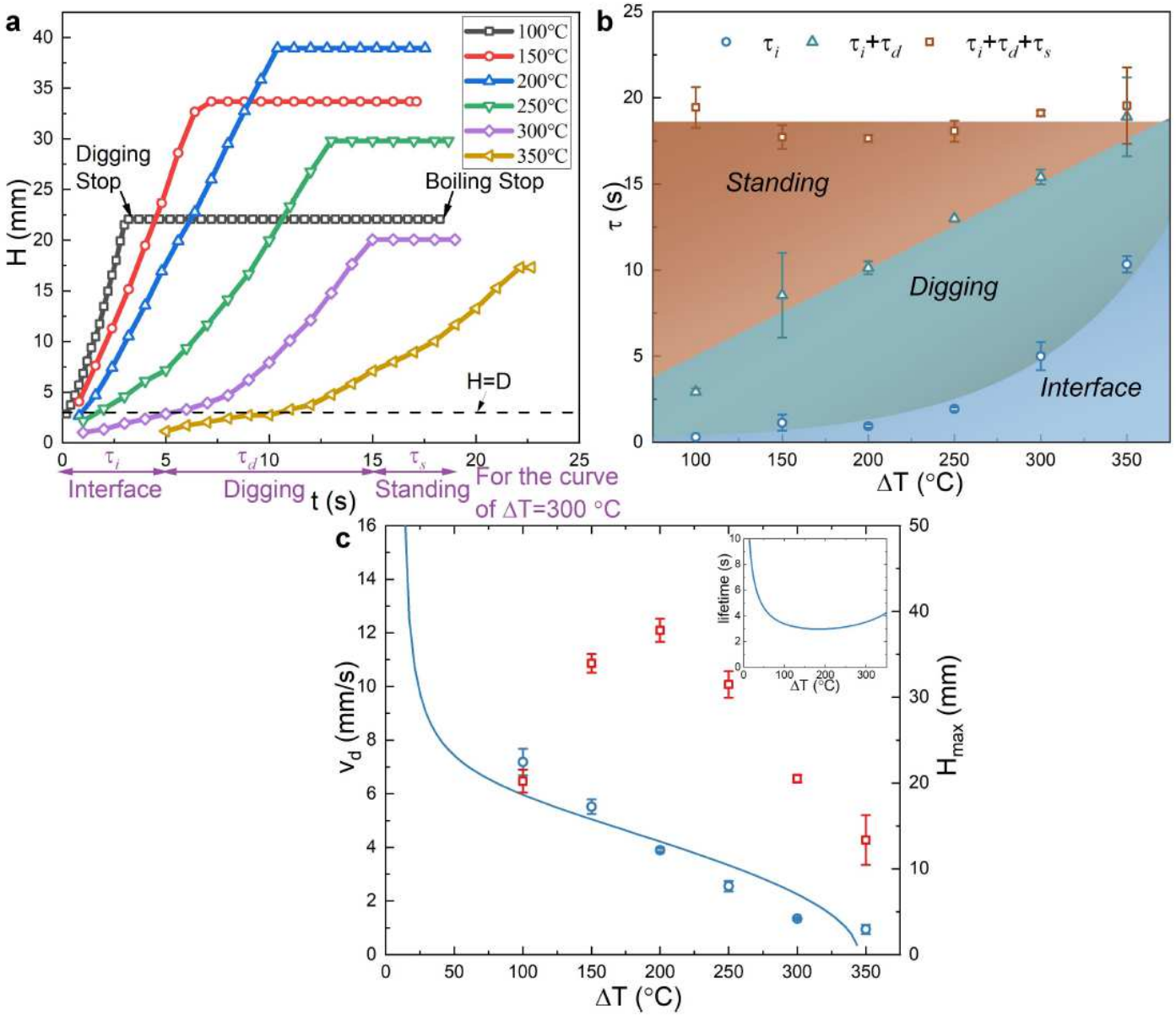

Figure 3

(a) Height reached by the droplet as a function of time for different temperatures between 200 and 450°C (see Legend). Three steps can be identified: the time to cross the interface τi, the deep digging process during the time τd and the stand-by state during τs. In red, the different step durations are represented for the case Tb = 400°C. (b) Distribution of the duration of the different steps (τi, τd and τs are the black squares, the red circles and the blue triangles respectively) during the digging process as a function of the

superheat ΔT. The total duration of the process remains constant. The time to cross the interface increases with the superheat. On the other hand, since the standing time linearly increases with ΔT, the digging duration is maximum when ΔT = 250° C. (c) The maximum depth reached by the droplet is presented as a function of the temperature (red squares). A maximum depth is reached for ΔT =300 °C. The speed during the digging process is also presented as a function the granular bed superheat (blue bullets). The speed keeps on decreasing with the temperature. The curve correspond to the model presented in the discussion section for rrug =70 µm, kSiC =0.70 W/m/K.

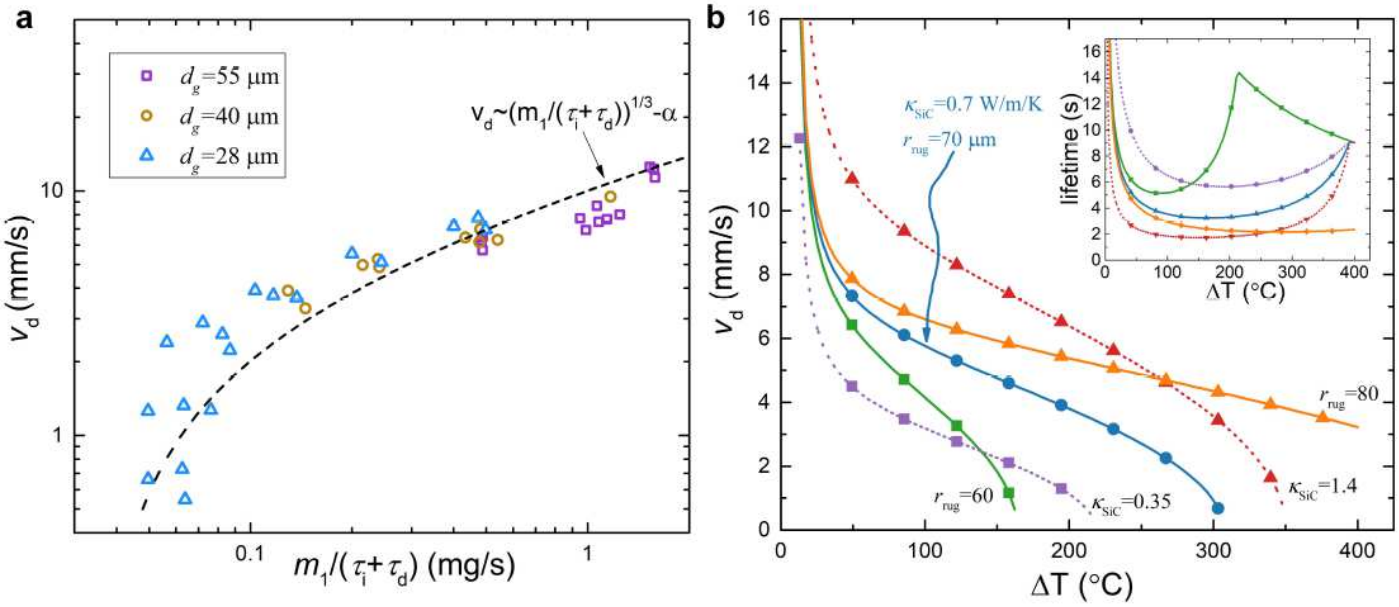

Figure 4

(a) Digging speed as a function of the experimental vapour production namely m1=(τi +τd). The dashed curve correspond to a fit by a power law 1/3. (b) Digging speed and vaporisation lifetime (inset) determined by the model as a function of the superheat ΔT. The best fit case, rrug = 70 µm and kSiC=0.7 W/m/K (continuous blue curve decorated with bullets) is compared to different values of rrug and kSiC. The continuous curves correspond to rrug=60 and 80 µm (green squares and orange triangles respectively) kSiC=0.7 W/m/K. The dashed curves correspond to kSiC=0.35 and 1.4 W/m/K (purple squares and red triangles respectively) rrug=70 µm.

Supplementary Files

This is a list of supplementary files associated with this preprint. Click to download.

- SupplementalInformation.pdf
- MovieS1.mp4
- MovieS2.mp4
- MovieS3.mp4

- MovieS4.mp4
- MovieS5.mp4
- MovieS6.mp4
- MovieS7.mp4